Spectroscopic evidence for limited carrier hopping interaction in amorphous ZnO thin film

Deok-Yong Cho,[1,a)] Jeong Hwan Kim,[2] Kwang Duk Na,[2] Jaewon Song,[2] Cheol Seong Hwang,[2,a)] Byeong-Gyu Park,[3] Jae-Young Kim,[3] Chul-Hee Min,[4] and Se-Jung Oh[4]

[1]*Department of Physics, Sungkyunkwan University, Suwon 440-746, Republic of Korea*
[2]*Department of Materials Science and Engineering, Inter-university Semiconductor Research Center, Seoul National University, Seoul 151-744, Republic of Korea*
[3]*Pohang Accelerator Laboratory, Pohang University of Science and Technology, Pohang 790-784, Republic of Korea*
[4]*CSCMR & FPRD, Department of Physics and Astronomy, Seoul National University, Seoul 151-747, Republic of Korea*

(Received 13 November 2009; accepted 25 November 2009; published online 28 December 2009)

The electronic structure of amorphous ZnO film (*a*-ZnO) was examined by O *K*- and Zn L_3-edge x-ray absorption spectroscopy and valence band photoemission spectroscopy. Comparative studies of *a*-ZnO and a wurtzite ZnO (*w*-ZnO) revealed a decrease in Zn 4*s*-O 2*p* hybridization strength and the localization of Zn 4*s* band as a consequence of local structural disorder, indicating limited electron hopping interactions in *a*-ZnO. The 0.1 eV higher Fermi-level of *a*-ZnO compared to *w*-ZnO suggests that the electrical properties of *a*-ZnO are different from those in *w*-ZnO due to structural disorder, even in the absence of impurities or grain boundaries. © *2009 American Institute of Physics*. [doi:10.1063/1.3275738]

Zinc-oxide-based oxide semiconductors have been highlighted as a channel material in thin film transistors for transparent electronics.[1,2] The electrical conductivity in the primitive material, zincite (ZnO),[3] is provided mainly by electron occupation of the Zn 4*s* conduction band (CB) (Ref. 4) over a large bandgap (>3 eV) accompanied by shallow gap states due to the inclusion of hydrogen ions or oxygen vacancies.[5,6] Since the electron mobility in polycrystalline ZnO is limited significantly by dislocations or impurities at the grain boundaries, it has been believed that an amorphous phase of ZnO, where there are no grain boundaries, would be desirable as a channel material in high-speed transparent electronic devices.[7–9]

However, even in the absence of grain boundaries, the electron mobility in a disordered system can be decreased by the random distortion of atomic arrangements. The decrease in mobility at the band edges in amorphous metallic/semiconducting systems is well understood to be a consequence of a loss of lattice periodicity.[10] However, in the case of ZnO, which is close to an insulator (with a bandgap ~3.4 eV), this concept is not applicable because the carrier density in ZnO is too low to form an extended conduction, so the mobility is influenced significantly by local hopping interactions between the adjacent atoms.

This letter provides spectroscopic evidence that the intersite Zn 4*s*-O 2*p* hopping interaction in amorphous ZnO (*a*-ZnO) is truly weaker than that in crystalline (wurtzite) ZnO (*w*-ZnO). The strengths of the Zn–O hopping interactions were represented by the hybridization strengths of the Zn $4s \oplus$ O 2*p* unoccupied states, which were deduced from O *K*-edge ($1s \rightarrow 2p$) x-ray absorption spectroscopy (XAS). The consequent localization of the Zn 4*s* state was also confirmed by Zn L_3-edge XAS (Zn $2p_{3/2} \rightarrow s/d$).

A 2 nm thick *a*-ZnO film was deposited on a Si (001) substrate at room temperature by rf magnetron sputtering using a ZnO target without an additional oxygen gas supply. The input rf power and working pressure were 200 W and 0.7 Pa, respectively. The amorphousness of the film was confirmed by glancing angle x-ray diffraction (XRD), and was also self-evident in XAS. A 50 nm thick *w*-ZnO film was deposited under the same conditions for comparison. The θ-2θ XRD patterns confirmed that the film had crystallized in the wurtzite structure with the *c*-axis being oriented along the direction normal to the surface. The O *K*-edge (~530 eV) and Zn L_3-edge (~1020 eV) XAS and photoemission spectroscopy were performed at the 2A beamline in the Pohang Light Source (PLS).

Figure 1 shows the O *K*-edge XAS spectra of the *a*-ZnO

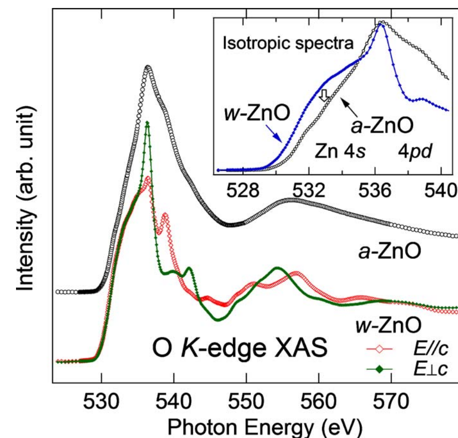

FIG. 1. (Color online) The O *K*-edge XAS spectra of the *a*- and *w*-ZnO films. Features near the conduction band edge in the isotropic spectra $[\{2\times(E\perp c)+(E\parallel c)\}/3]$ are magnified in the inset. A decrease of feature relevant to the Zn 4*s*-O 2*p* hybridization was clearly observed.

[a)]Authors to whom correspondence should be addressed. Electronic addresses: dycho@skku.edu and cheolsh@snu.ac.kr.

 © 2009 American Institute of Physics

Author complimentary copy. Redistribution subject to AIP license or copyright, see http://apl.aip.org/apl/copyright.jsp

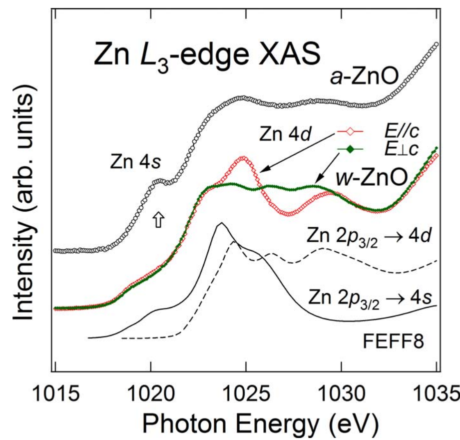

FIG. 2. (Color online) The Zn L_3-edge XAS spectra of the *a*- and *w*-ZnO films with the simulation results for the isotropic $2p_{3/2} \rightarrow s/d$ transitions in *w*-ZnO. A prominence of Zn 4*s* features in the *a*-ZnO, which reflects the Zn 4*s* localization, was highlighted by the arrow.

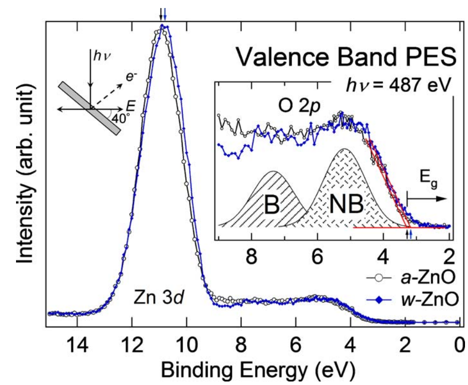

FIG. 3. (Color online) VB photoemission spectra of the *a*- and *w*-ZnO films obtained using photon energy of 487 eV. Overall binding energy shift in *a*-ZnO spectrum reflects the increased E_F by +0.1 eV. The VB features for the bonding and nonbonding states are magnified in the inset. The measurement geometry is also depicted.

and *w*-ZnO films. For the assignments of the features, the spectra were obtained using two perpendicular incident beam polarization. The spectra of *w*-ZnO showed large polarization dependence above a photon energy of 535 eV, indicating that the features at 530–535 eV and above 535 eV should be assigned to the O 2*p* states that hybridize with the isotropic Zn 4*s* states and anisotropic Zn 4*pd* states, respectively. In contrast, the spectra of *a*-ZnO showed no polarization dependence, manifesting the amorphousness of the film. The spectra of *a*- and *w*-ZnO showed a significant difference, even in line shape of the isotropic spectra $\{(E\|c)+2\times(E\perp c)\}/3$, which is highlighted in the inset. This evidences the difference in the unoccupied states of the two films. The intensity of the Zn $4s\oplus$O 2*p* feature of *a*-ZnO in the CB structure was ~10% lower than of *w*-ZnO as shown in the inset, indicating a decrease in the Zn 4*s*-O 2*p* hybridization strength. The apparent increase in the offset photon energy in the isotropic spectra of *a*-ZnO, compared to *w*-ZnO, can be resolved by considering that the O *K*-edge XAS shows only parts of the CB states that hybridize with the O 2*p* states. A significant decrease in hybridization strength occurs, particularly near the CB edge, resulting in an apparent increase in offset energy. The CB edge energy and bandgap should decrease if the system becomes amorphous as in the case of Si.[11,12]

Instead of the O *K*-edge XAS, in which the Zn 4*s* features were observed indirectly through Zn 4*s*-O 2*p* hybridization, the Zn L_3-edge XAS can probe the Zn 4*s* states directly through the Zn $2p_{3/2} \rightarrow$Zn s/d transitions. However, in this case, the core hole at the photon-absorbing Zn ion could possibly interact with the valence electrons at the same ion so as to reflect the perturbed Zn 4*s* states rather than the genuine 4*s* states. Figure 2 shows the Zn L_3-edge XAS spectra of the *a*- and *w*-ZnO films. The solid (dashed) lines, which show the theoretical isotropic $2p_{3/2} \rightarrow 4s$ (4*d*) spectra of the *w*-ZnO simulated using FEFF8 CODE,[13] were added to make the peak assignments clearer. In the XAS simulation, a time-dependent local density approximation option was used to account for the 2*p* core-hole and valence screening effects.[14] The effect of this shallow $2p_{3/2}$ core-level was negligible on this material,[14] suggesting that the spectra approximately reflect the CB structures. The simulated spectra clearly show that the near-edge features (~1020 eV) are dominated by Zn 4*s* bands, while the features above 1025 eV are due mainly to the Zn 4*d* bands.

The CB edge feature (highlighted by the arrow) in the spectrum of *a*-ZnO is not smaller than that of *w*-ZnO. Rather it appears to have slightly higher intensity than that of *w*-ZnO. Thus, the Zn 4*s* density of states (DOS) itself in *a*-ZnO does not decrease compared to that of *w*-ZnO. This confirms that the decrease in the intensity of the Zn 4*s* $\oplus$O 2*p* features in the O *K*-edge XAS (Fig. 1) must be due to a decrease in Zn 4*s*-O 2*p* hybridization not in the Zn 4*s* DOS itself. Therefore, the salient Zn 4*s* features in the Zn L_3-edge XAS spectrum of *a*-ZnO, indicates the localization of the Zn 4*s* wave function due to the orbital dehybridization. The decreased Zn–O hybridization strength suggests that local hopping interactions between the adjacent Zn and O ions in *a*-ZnO are weaker than those in *w*-ZnO even in the absence of a dopant or grain boundaries in the film.

The Zn 4*s* localization can slightly enhance the Zn 4*s* DOS (Fig. 2) near the CB through decoupling it from the higher-energy Zn states such as the Zn 4*pd* states. The enhanced CB DOS can further influence the Fermi-level (E_F) and band alignment of ZnO films in an actual transistor depending on the degree of amorphousness. A change in E_F was observed in the valence band (VB) photoemission spectra. Figure 3 shows the VB photoemission spectra of the two films obtained at a photon energy of 487 eV. In order to obtain isotropic spectra, the samples were tilted by ~40° off from the direction of incident light as shown in the figure. The large features at a binding energy (BE) of ~10.8 eV originated from the Zn 3*d* level and the smaller features near BE<9 eV were assigned to the O 2*p* occupied states. The O 2*p* features near BEs ~8 eV consist of O 2*p* "bonding" states that hybridize mainly with the Zn 4*sp* orbitals, while those near the VB edge (~4 eV) are mainly the nonbonding O 2*p* states.[15] The Zn 3*d* BE of the *a*-ZnO film is slightly higher than that of the *w*-ZnO film by +0.1 eV. In addition, the BEs of the O 2*p* states near the VB edges (~4 eV) showed a slight difference by the same amount of +0.1 eV. This suggests that the slight shift in BE did not originate from a change in the chemistry in ZnO because the BE shifts of the Zn 3*d* and O 2*p* would have opposite signs to each other. Rather, the BE shift was caused by a difference in E_F; a positive E_F shift induces a higher-BE shift in the photoemission spectra because the BE is obtained as the energy

Author complimentary copy. Redistribution subject to AIP license or copyright, see http://apl.aip.org/apl/copyright.jsp

difference from the E_F. The absence of a chemical shift suggests that the possible formation of interface states such as the (Zn,Si)O was suppressed. The 0.1 eV higher E_F in the *a*-ZnO film compared to the *w*-ZnO film might be relevant to the enhanced CB features shown in Fig. 2, as in the case of donor states in semiconductors. The slight increase in intensity of the feature near BE ~9 eV in the case of *a*-ZnO, might reflect the raised O 2*p* projected DOS due to the weaker Zn 4*s*-O 2*p* hybridization, since the photoionization cross-section (or probability) of the O 2*p* orbital is higher than that of the Zn 4*s* orbital at $h\nu=487$ eV.

The decrease in Zn–O hybridization strength possibly originates from the weakened long-range structural orders in *a*-ZnO. Broken structural order might isolate the local Zn–O clusters and hinder the electron hopping interactions between the clusters by reducing the overlap integral of the orbital wave functions. Orbital hybridization in a Zn–O cluster can occur only when the symmetry of the central atomic orbital coincides with that of the surrounding ligand orbital clouds. Therefore, the enhanced disorder in the local Zn–O coordination will decrease the hybridization strength via the orbital symmetry mismatch and consequently the intersite hopping probability will decrease. This will result in the localization of CB states and increase the effective mass of the electrons. Eventually, the electron mobility can be reduced because the mobility in this insulator-like low-carrier regime is determined by the effective mass or localization of the conduction electrons. Further studies examining the electrical properties and electronic structure in the ZnO system with various degrees of amorphousness will be needed to clarify the interconnection between the physical properties.

In conclusion, amorphous ZnO showed lower Zn 4*s*-O 2*p* hybridization strength and localized Zn 4*s* bands compared to crystalline ZnO. This indicates a decrease in electron hopping interactions in the amorphized ZnO. The 0.1 eV higher E_F further suggests that the electrical properties of amorphous ZnO may be different from those in crystalline ZnO due to structural disorders, even in the absence of impurities or grain boundaries.

This study was supported by the Samsung Advanced Institute of Technology, and the KOSEF through the WCU program (Grant No. R31-2008-000-10075-0) and the Acceleration Research Program (Grant No. R17-2008-033-01000-0). The experiment at the PLS was supported in part by MEST and POSTECH.

[1]H. Hosono, J. Non-Cryst. Solids **352**, 851 (2006).
[2]*Zinc Oxide - A Material for Micro and Optoelectronic Applications*, edited by N. H. Nickel and E. Terukov (Springer, New York, 2005).
[3]*Transparent Conductive Zinc Oxide: Basics and Applications in Thin Film Solar Cells*, edited by K. Ellmer, A. Klein, and B. Rech (Springer, New York, 2008).
[4]M. Goano, F. Bertazzi, M. Penna, and E. Bellotti, J. Appl. Phys. **102**, 083709 (2007).
[5]C. Yang, X. M. Li, Y. F. Gu, W. D. Yu, X. D. Gao, and Y. W. Zhang, Appl. Phys. Lett. **93**, 112114 (2008).
[6]A. Janotti and C. G. Van de Walle, Nature Mater. **6**, 44 (2007).
[7]H.-H. Hsieh and C.-C. Wu, Appl. Phys. Lett. **91**, 013502 (2007).
[8]R. Martins, P. Barquinha, I. Ferreira, L. Pereira, G. Gonçalves, and E. Fortunato, J. Appl. Phys. **101**, 044505 (2007).
[9]S. T. Tan, B. J. Chen, X. W. Sun, W. J. Fan, H. S. Kwok, X. H. Zhang, and S. J. Chua, J. Appl. Phys. **98**, 013505 (2005).
[10]P. W. Anderson, Phys. Rev. **109**, 1492 (1958).
[11]G. D. Cody, T. Tiedje, B. Abeles, B. Brooks, and Y. Goldstein, Phys. Rev. Lett. **47**, 1480 (1981).
[12]J. M. Khoshman and M. E. Kordesch, Thin Solid Films **515**, 7393 (2007).
[13]A. L. Ankudinov, B. Ravel, J. J. Rehr, and S. D. Conradson, Phys. Rev. B **58**, 7565 (1998).
[14]V. Mauchamp, M. Jaouen, and P. Schattschneider, Phys. Rev. B **79**, 235106 (2009).
[15]J. A. Tossell, Inorg. Chem. **16**, 2944 (1977).

Author complimentary copy. Redistribution subject to AIP license or copyright, see http://apl.aip.org/apl/copyright.jsp